Journal of Marine Science and Technology

Volume 21 | Issue 3 Article 9

A PISTON-TYPE POROUS WAVE ENERGY CONVERTER THEORY

Ching-Yun Yueh
Department of Harbor and River Engineering, National Taiwan Ocean University, Keelung, Taiwan, R.O.C.

Shih-Hsuan Chuang
Department of Harbor and River Engineering, National Taiwan Ocean University, Keelung, Taiwan, R.O.C, shoverlaychuang@hotmail.com

Journal of Marine Science and Technology, Vol. 21, No. 3, pp. 309-317 (2013)
DOI: 10.6119/JMST-012-0518-1

A PISTON-TYPE POROUS WAVE ENERGY CONVERTER THEORY

Ching-Yun Yueh and Shih-Hsuan Chuang

Key words: wave energy, vertical porous plate, wave trapping, resonance.

ABSTRACT

This study investigates the performance of a piston-type porous wave energy converter (PTPWEC), which consists of a solid wall, a vertical porous plate, a transmission bar, a rigid block constrained by rollers, a spring, and a damper. The PTPWEC is subjected to dynamic external loading by wave actions. To simulate this dynamic system, a mathematical model is used with a single-degree-of-freedom (SDOF) system. Linear wave theory governs the entire fluid domain, which is divided into two regions by the vertical porous plate. Darcy's law is applied to flow through the porous plate. Finally, this investigation employs an eigenfunction expansion to yield a solution. A series of numerical experiments are conducted to determine the hydrodynamic added mass, radiation damping, converter response, and instantaneous mechanical power obtained from the wave.

I. INTRODUCTION

Since the First World War, petroleum has become the most important modern source of energy. As a nonrenewable source, its supply is intrinsically limited. The two oil crises in the 1970s and concerns about global warming in the last decade reflect concerns about the extensive utilization of fossil fuels. The increasing public awareness of the problem has stimulated advances in renewable energy development [10, 11].

An important characteristic of ocean waves is their high energy density, which is the highest among renewable energy sources. Worldwide wave power is estimated at 90×10^{15} W, presenting a renewable resource of 10^{12}-10^{13} W [16]. Moreover, the International Energy Agency [12] estimated that wave energy could eventually provide over 10% of the world's current electricity supply.

Paper submitted 09/19/11; revised 05/03/12; accepted 05/18/12. Author for correspondence: Shih-Hsuan Chuang (e-mail: shoverlaychuang@hotmail.com).
Department of Harbor and River Engineering, National Taiwan Ocean University, Keelung, Taiwan, R.O.C.

Previous studies (e.g., [2, 8-10, 15, 19]) have introduced and compared several wave energy converters (WECs) as proposed designs for power-take-off (PTO) mechanisms. This study investigates the performance of a piston-type porous wave energy converter (PTPWEC) consisting of a solid wall, a vertical porous plate, a transmission bar, a rigid block, a spring, a damper, and several rollers (see Fig. 1).

Investigation of the vertical porous plate in coastal engineering began many years ago. Chwang and Dong [5] linearized the problem of wave reflection from a thin barrier with fine pores, solving the system by an eigenfunction expansion method. The authors found that the reflected wave amplitude was minimized when the distance between the porous barrier and the chamber end wall was equal to an odd multiple of the quarter-wavelength of the incident wave. Twu and Lin [18] extended Chwang's method to evaluate wave reflection from a wave absorber containing a finite number of vertical porous plates with various porosities. The wave absorber was most efficient when the porosity of the plates was arranged in progressively decreasing order from the front of the absorber to the back. Several researchers have considered vertical porous plates as flexible structures (e.g., [20, 21, 23]). Others have focused on the interaction between water waves and composite structures with a finite number of porous plates (e.g., [13, 17, 22, 25, 26]).

Caska and Finnigan [3] proposed that a good wavemaker is also a good wave absorber. Chwang and Li [6] and Chwang [4] defined porous plates or paddles using a porous-effect parameter and obtained analytical solutions. They found that resonance occurs when porous plates are located at wave antinodes. In the porous wavemaker system, the porous plate functions as an energy supplier; hence, the specific kinematic properties of its movement (including the period, stroke, velocity, and acceleration) can be given. For the WEC problem, these properties depend on the design of the PTO mechanism.

Lastly, other authors [1, 14] have used a single-degree-of-freedom (SDOF) system to simulate the dynamic system represented by a vertical impermeable plate in the wave-body interaction problem.

The present study extends Chwang's method by introducing a SDOF system to analyze the PTPWEC. Analytical solutions were obtained for the added mass, the radiation damping, the reflection coefficient, the exerted force, the

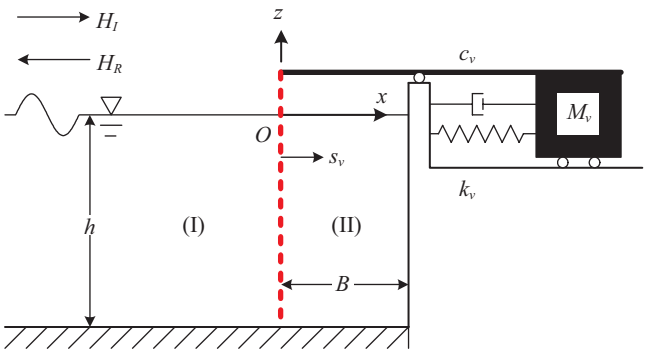

Fig. 1. Sketch of the modeled system.

motion response, and the corresponding instantaneous device power. Although certain assumptions were made to simplify the original conditions from a physical problem to yield the mathematical model, thus limiting the solutions to a reliant zone (e.g., a small-amplitude surface wave or a small plate displacement), this study explores the basic mechanics of wave-body interactions.

The next section describes the governing equations and boundary conditions. Section 3 presents the eigenfunction expansion method; Sections 4-7 explore the hydrodynamic added mass and radiation damping, the porous-plate response, the wave-exerted force, and the instantaneous power, respectively. Section 8 presents our conclusions.

II. GOVERNING EQUATIONS AND BOUNDARY CONDITIONS

We first consider the interaction between a PTPWEC and a gravity wave train. The PTPWEC consists of a solid wall, a vertical porous plate, a transmission bar, a rigid block constrained by rollers, a weightless spring, and a damper. The transmission bar horizontally connects the vertical porous plate and the rigid block. The weightless spring of stiffness k_v (per unit width) and damper (per unit width) are both planted between the solid wall and the rigid block. A semi-infinite fluid region of constant depth, h, is connected to the PTPWEC. Fig. 1 displays a sketch of the configuration. A SDOF system is used to simulate the dynamic system. The entire mass M_v of this dynamic system per unit width was included in the rigid block, constrained by rollers to move horizontally along the solid wall. In this system, the total damping force (including the inherent and applied damping) is the product of the damping constant c_v and the velocity of the porous plate. The width of the wave-absorbing chamber is B, and the single displacement coordinate s_v completely defines the position of the vertical porous plate. The ratio of the plate thickness to the length scale of the wave motion within the porous medium is sufficiently small that the plate thickness can be neglected. A Cartesian coordinate system is used to represent the problem: the origin O of the rectangular coordinate system is at the still water line; the x-axis points horizontally in the direction of wave propagation, and the z-axis points vertically upward. The vertical porous plate divides the fluid domain into two regions: (I) The exterior region ($x \le 0$, $-h \le z \le 0$) and (II) the interior region within the wave-absorbing chamber ($0 \le x \le B$, $-h \le z \le 0$).

For an incompressible fluid and nonrotational motion, velocity potentials $\Phi^j(x, z, t)$ describe the wavefield and satisfy the Laplace equation within the fluid region:

$$\nabla^2\Phi^j(x,z,t)=\frac{\partial^2\Phi^j}{\partial x^2}+\frac{\partial^2\Phi^j}{\partial z^2}=0,\ \ j=\mathrm{I,\ II} \tag{1}$$

where ∇^2 denotes the Laplace operator, t is time, and the superscript j represents the variables with respect to region (j).

Assuming constant air pressure, the linearized boundary condition on the free surface is obtained from the free surface kinematic and dynamic boundary conditions:

$$\frac{\partial^2\Phi^j}{\partial t^2}+g\frac{\partial\Phi^j}{\partial z}=0 \ \text{ on } \ z=0,\ \ j=\mathrm{I,\ II} \tag{2}$$

where g is gravitational acceleration.

The boundary condition on the impermeable seabed and the fixed solid wall are provided by Eqs. (3) and (4), respectively:

$$\frac{\partial\Phi^j}{\partial z}=0 \ \text{ on } \ z=-h,\ \ j=\mathrm{I,\ II} \tag{3}$$

$$\frac{\partial\Phi^{\mathrm{II}}}{\partial x}=0 \ \text{ on } \ x=B \tag{4}$$

Under a wave attack, the porous plate of this WEC moves horizontally. The plate is assumed to be a rigid homogeneous porous medium [4].

$$\frac{\partial\Phi^{\mathrm{I}}}{\partial x}=\frac{\partial\Phi^{\mathrm{II}}}{\partial x}=\frac{k_0G}{\rho\sigma}(P^{\mathrm{I}}-P^{\mathrm{II}})+U_v \ \text{ on } \ x=0 \ \text{ and } \ -h\le z\le 0 \tag{5}$$

where ρ denotes the fluid density, σ represents the angular frequency ($\sigma=2\pi/T$, where T is the wave period), G is the complex ($G = G_r + iG_i$) porous-effect parameter [24], k_0 is the wavenumber of the incident wave satisfying the dispersion relation in Eq. (15), P^{I} and P^{II} respectively represent the hydrodynamic pressures on the left and right sides of the movable porous boundary, and $U_v = ds_v/dt$ denotes the porous plate velocity.

The motion equation for the porous plate subjected to an external source of dynamic loading from the attack of the wave is written in terms of the complex displacement $s_v(t)$ as follows [1, 7]:

$$M_v\ddot{s}_v(t)+c_v\dot{s}_v(t)+k_vs_v(t)=F(t) \tag{6}$$

where $F(t)$ represents the force exerted on the porous plate from the wave per unit width of the plate.

The hydrodynamic pressures P^{I} and P^{II} are related to the velocity potentials through the linearized Bernoulli equation:

$$P^j = -\rho \frac{\partial \Phi^j}{\partial t},\ j = \mathrm{I, II} \text{ on } x = 0 \text{ and } -h \le z \le 0 \tag{7}$$

Based on linear wave theory, we assume that the velocity potential, the hydrodynamic pressure, and the porous plate displacement are all periodic functions of t with a time factor $\exp(-i\sigma t)$:

$$\Phi^j = \phi^j(x, z)\exp(-i\sigma t),\ j = \mathrm{I, II} \tag{8}$$

$$P^j = p^j(x, z)\exp(-i\sigma t),\ j = \mathrm{I, II} \tag{9}$$

$$s_v = \Lambda \exp(-i\sigma t) \tag{10}$$

where ϕ denotes the spatial velocity potential, p is the spatial hydrodynamic pressure, and Λ represents the complex displacement amplitude, which is here assumed to be small in comparison with the undisturbed water depth.

Substituting Eq. (10) into $U_v = ds_v/dt$, we obtain

$$U_v = \frac{ds_v}{dt} = -i\sigma\Lambda \exp(-i\sigma t) \tag{11}$$

By substituting Eqs. (8), (9) and (11) into Eq. (5), the boundary conditions for the movable porous plate can be rewritten as spatial variables:

$$\frac{\partial \phi^{\mathrm{I}}}{\partial x} = \frac{\partial \phi^{\mathrm{II}}}{\partial x} = \frac{k_0 G}{\rho\sigma}(p^{\mathrm{I}} - p^{\mathrm{II}}) - i\sigma\Lambda \text{ on } x = 0 \text{ and } -h \le z \le 0 \tag{12}$$

III. EIGENFUNCTION EXPANSION METHOD

We next construct eigensolutions for the boundary-value problem (BVP) described in the previous section. By separating the variables, the spatial velocity potentials ϕ^j (j = I, II) satisfying the radiation condition and Eqs. (1)-(4) are obtained:

$$\phi^{\mathrm{I}}(x, z) = A_0 \frac{\cosh k_0(h+z)}{\cosh k_0 h}\exp(ik_0 x) + B_0 \frac{\cosh k_0(h+z)}{\cosh k_0 h}\exp(-ik_0 x) + \sum_{m=1}^{\infty} B_m \frac{\cos k_m(h+z)}{\cos k_m h}\exp(k_m x)$$
$$\text{for } x \le 0 \text{ and } -h \le z \le 0 \tag{13}$$

$$\phi^{\mathrm{II}}(x, z) = C_0 \frac{\cosh k_0(h+z)}{\cosh k_0 h}\cos k_0(x - B) + \sum_{m=1}^{\infty} C_m \frac{\cos k_m(h+z)}{\cos k_m h}\cosh k_m(x - B)$$
$$\text{for } x \le 0 \le B \text{ and } -h \le z \le 0 \tag{14}$$

where A_0 is the incident wave constant relating to the incident wave amplitude; B_m and C_m (m = 0, 1, 2, …) are undetermined coefficients; and k_0 and k_m (m = 1, 2, 3, …) satisfy the dispersion relation:

$$\sigma^2 = g k_0 \tanh k_0 h \tag{15a}$$

$$\sigma^2 = -g k_m \tan k_m h,\ m = 1, 2, 3, \ldots \tag{15b}$$

By substituting Eqs. (8), (13), and (14) into Eq. (7), the spatial hydrodynamic pressures on both sides of the porous plate (p^{I} and p^{II}) can be written as follows:

$$p^{\mathrm{I}} = i\sigma\rho\left[(A_0 + B_0)\frac{\cosh k_0(h+z)}{\cosh k_0 h} + \sum_{m=1}^{\infty} B_m \frac{\cos k_m(h+z)}{\cos k_m h}\right]$$
$$\text{for } -h \le z \le 0 \tag{16}$$

$$p^{\mathrm{II}} = i\sigma\rho\left[C_0 \frac{\cosh k_0(h+z)}{\cosh k_0 h}\cos k_0 B + \sum_{m=1}^{\infty} C_m \frac{\cos k_m(h+z)}{\cos k_m h}\cosh k_m B\right] \text{ for } -h \le z \le 0 \tag{17}$$

After substituting Eqs. (13), (16), and (17) into Eq. (12) and multiplying both sides by $\cosh k_0(h + z)$ and $\cos k_m(h + z)$, we integrate Eq. (12) from $-h$ to 0. The orthogonal relationships yield the following equations:

$$(1+G)B_0 - (G\cos k_0 B)C_0 = (1-G)A_0 + \frac{\sigma\Lambda}{N_0 k_0} \tag{18}$$

$$(k_0 G + ik_m)B_m - (k_0 G\cosh k_m B)C_m = \frac{\sigma\Lambda}{N_m},\ m = 1, 2, 3, \ldots \tag{19}$$

where

$$N_0 = \frac{1}{2}\left(1 + \frac{2k_0 h}{\sinh 2k_0 h}\right) \tag{20}$$

$$N_m = \frac{1}{2}\left(1 + \frac{2k_m h}{\sin 2k_m h}\right),\ m = 1, 2, 3, \ldots \tag{21}$$

Similar to the above process, substituting Eqs. (14), (16), and (17) into Eq. (12), multiplying both sides by $\cosh k_0(h + z)$ and $\cos k_m(h + z)$, and then integrating z from $-h$ to 0 yields the following equations:

$$GB_0 - (G\cos k_0B - i\sin k_0B)C_0 = -GA_0 + \frac{\sigma\Lambda}{N_0k_0} \tag{22}$$

$$k_0GB_m - (k_0G\cosh k_mB + ik_m\sinh k_mB)C_m = \frac{\sigma\Lambda}{N_m},\ m = 1, 2, 3, \ldots \tag{23}$$

Using Eqs. (18) and (22), B_0 and C_0 may be rewritten in terms of A_0 and Λ:

$$B_0 = \frac{Ge^{ik_0B} - i\sin k_0B}{Ge^{-ik_0B} - i\sin k_0B}A_0 - \frac{i\sin k_0B}{Ge^{-ik_0B} - i\sin k_0B}\cdot\frac{\sigma\Lambda}{N_0k_0} \tag{24}$$

$$C_0 = \frac{2G}{Ge^{-ik_0B} - i\sin k_0B}A_0 - \frac{1}{Ge^{-ik_0B} - i\sin k_0B}\cdot\frac{\sigma\Lambda}{N_0k_0} \tag{25}$$

Similarly, B_m and C_m (m = 1, 2, 3, …) may be rewritten in terms of Λ by Eqs. (19) and (23):

$$B_m = \frac{\sinh k_mB}{k_0Ge^{k_mB} + ik_m\sinh k_mB}\cdot\frac{\sigma\Lambda}{N_m},\ m = 1, 2, 3, \ldots \tag{26}$$

$$C_m = \frac{-1}{k_0Ge^{k_mB} + ik_m\sinh k_mB}\cdot\frac{\sigma\Lambda}{N_m},\ m = 1, 2, 3, \ldots \tag{27}$$

By integrating the hydrodynamic pressure distribution on the face of the porous plate, the exerting force $F(t)$ can be expressed as

$$F(t) = \int_{-h}^{0}(P^{\mathrm{I}} - P^{\mathrm{II}})dz \ \text{ on } \ x = 0 \tag{28}$$

Introducing Eqs. (9), (16), and (17) into Eq. (28) yields:

$$F(t) = i\sigma\rho\left[(A_0 + B_0 - C_0\cos k_0B)\frac{\tanh k_0h}{k_0} + \sum_{m=1}^{\infty}(B_m - C_m\cosh k_mB)\frac{\tan k_mh}{k_m}\right]\exp(-i\sigma t) \tag{29}$$

which can be introduced into the particular solution, i.e., the steady-state harmonic response, of Eq. (6):

$$\Lambda\exp(-i\sigma t) = \frac{F(t)}{k_v - \sigma^2M_v - i\sigma c_v} \tag{30}$$

yielding

$$\Lambda = \frac{2\sigma\rho\sin k_0B\tanh k_0h}{\left[k_v - \sigma^2(M_v + M_A) - i\sigma(c_v + R_D)\right]\left(Ge^{-ik_0B} - i\sin k_0B\right)k_0}A_0 = C_\Lambda A_0 \tag{31}$$

where M_A and R_D are the hydrodynamic added mass and radiation damping respectively, expressed as

$$M_A = \rho\left\{\frac{\tanh k_0h}{N_0{k_0}^2}\cdot\frac{G_i - \sin k_0B\cos k_0B}{(G_r + \sin^2 k_0B)^2 + (G_i - \sin k_0B\cos k_0B)^2} + \sum_{m=1}^{\infty}\frac{\tan k_mh}{N_mk_m}\cdot\frac{k_0G_i + 0.5k_m(1 - e^{-2k_mB})}{(k_0G_r)^2 + \left[k_0G_i + 0.5k_m(1 - e^{-2k_mB})\right]^2}\right\} \tag{32}$$

$$R_D = \sigma\rho\left\{\frac{\tanh k_0h}{N_0{k_0}^2}\cdot\frac{G_r + \sin^2 k_0B}{(G_r + \sin^2 k_0B)^2 + (G_i - \sin k_0B\cos k_0B)^2} + \sum_{m=1}^{\infty}\frac{\tan k_mh}{N_mk_m}\cdot\frac{k_0G_r}{(k_0G_r)^2 + \left[k_0G_i + 0.5k_m(1 - e^{-2k_mB})\right]^2}\right\} \tag{33}$$

Substituting Eq. (31) into Eqs. (24)-(27), we obtain the following:

$$B_0 = C_{B0}A_0 \tag{34}$$

$$C_0 = C_{C0}A_0 \tag{35}$$

$$B_m = C_{Bm}A_0,\ m = 1, 2, 3, \ldots \tag{36}$$

$$C_m = C_{Cm}A_0,\ m = 1, 2, 3, \ldots \tag{37}$$

where

$$C_{B0} = \frac{Ge^{ik_0B} - i\sin k_0B}{Ge^{-ik_0B} - i\sin k_0B} - \frac{i\sin k_0B}{Ge^{-ik_0B} - i\sin k_0B}\cdot\frac{\sigma C_\Lambda}{N_0k_0} \tag{38}$$

$$C_{C0} = \frac{2G}{Ge^{-ik_0B} - i\sin k_0B} - \frac{1}{Ge^{-ik_0B} - i\sin k_0B}\cdot\frac{\sigma C_\Lambda}{N_0k_0} \tag{39}$$

$$C_{Bm} = \frac{\sinh k_mB}{k_0Ge^{k_mB} + ik_m\sinh k_mB}\cdot\frac{\sigma C_\Lambda}{N_m},\ m = 1, 2, 3, \ldots \tag{40}$$

$$C_{Cm} = \frac{-1}{k_0Ge^{k_mB} + ik_m\sinh k_mB}\cdot\frac{\sigma C_\Lambda}{N_m},\ m = 1, 2, 3, \ldots \tag{41}$$

A gravity wave train propagating in the x-direction toward the porous plate is represented by

$$\eta_I = \zeta_0 \sin(k_0 x - \sigma t) \tag{42}$$

where η_I is the free-surface elevation of the incident wave, and ζ_0, a real-number constant, denotes the amplitude of η_I. We substitute Eqs. (8) and (13) into the linearized dynamic free surface boundary condition (DFSBC) $\eta = -\frac{1}{g}\frac{\partial \Phi}{\partial t}$ $(z = 0)$ to obtain the free-surface elevation for region (I). The two relationships can be written as

$$\zeta_R = \frac{\sigma}{g}|B_0| \tag{43}$$

$$\zeta_0 = -\frac{\sigma}{g} A_0 \tag{44}$$

where ζ_R, a real-number constant, is the amplitude of the reflected wave. The equation for the reflection coefficient R can be expressed as

$$R = \frac{\zeta_R}{\zeta_0} = -\frac{|B_0|}{A_0} \tag{45}$$

Following Eq. (44), we find that when ζ_0 is positive, A_0 is a negative real number. Introducing Eq. (34) into Eq. (45) yields Eq. (46):

$$R = |C_{B0}| \tag{46}$$

By substituting Eq. (44) into Eq. (31), the dimensionless complex amplitude Λ/ζ_0 representing the porous plate response is expressed as follows:

$$\frac{\Lambda}{\zeta_0} = -C_\Lambda \frac{g}{\sigma} = \frac{2\sin k_0 B \tanh k_0 h}{k_0 h \sqrt{a_1^{\,2} + b_1^{\,2}}\sqrt{a_2^{\,2} + b_2^{\,2}}} \cdot \exp\left[-i\tan^{-1}\left(\frac{b_1}{a_1}\right) - i\tan^{-1}\left(\frac{b_2}{a_2}\right)\right] \tag{47}$$

where

$$a_1 = k_0 h \tanh k_0 h(\overline{M_v} + \overline{M_A}) - \overline{k_v} \tag{48}$$

$$b_1 = (\overline{c_v} + \overline{R_D})\sqrt{k_0 h \tanh k_0 h} \tag{49}$$

$$a_2 = G_r \cos k_0 B + G_i \sin k_0 B \tag{50}$$

$$b_2 = G_i \cos k_0 B - (G_r + 1)\sin k_0 B \tag{51}$$

$$\overline{M_A} = \frac{M_A}{\rho h^2} = \frac{\tanh k_0 h}{(k_0 h)^2 N_0} \cdot \frac{G_i - \sin k_0 B \cos k_0 B}{(G_r + \sin^2 k_0 B)^2 + (G_i - \sin k_0 B \cos k_0 B)^2} + \sum_{m=1}^{\infty} \frac{\tan k_m h}{N_m k_m h} \cdot \frac{k_0 h G_i + 0.5 k_m h (1 - e^{-2k_m B})}{(k_0 h G_r)^2 + \left[k_0 h G_i + 0.5 k_m h (1 - e^{-2k_m B})\right]^2} \tag{52}$$

$$\overline{R_D} = \frac{R_D}{\rho\sqrt{gh^3}} = \sqrt{k_0 h \tanh k_0 h} \cdot \left\{ \frac{\tanh k_0 h}{(k_0 h)^2 N_0} \cdot \frac{G_r + \sin^2 k_0 B}{(G_r + \sin^2 k_0 B)^2 + (G_i - \sin k_0 B \cos k_0 B)^2} + \sum_{m=1}^{\infty} \frac{\tan k_m h}{N_m k_m h} \cdot \frac{k_0 h G_r}{(k_0 h G_r)^2 + \left[k_0 h G_i + 0.5 k_m h (1 - e^{-2k_m B})\right]^2} \right\} \tag{53}$$

where $\overline{M_v} = M_v / \rho h^2$, $\overline{c_v} = c_v / \rho\sqrt{gh^3}$ and $\overline{k_v} = k_v / \rho g h$.

Moreover, the wave-exerted force $F(t)$ is obtained by substituting Eqs. (44) and (34)-(37) into Eq. (29):

$$F(t) = -i\rho g \zeta_0 h \left[(1 + C_{B0} - C_{C0}\cos k_0 B)\frac{\tanh k_0 h}{k_0 h} + \sum_{m=1}^{\infty} (C_{Bm} - C_{Cm}\cosh k_m B)\frac{\tan k_m h}{k_m h} \right] \exp(-i\sigma t) \tag{54}$$

We can now derive the instantaneous power $P_W(t)$ from its physical definition.

$$P_W(t) = F(t) \cdot U_v(t) = \rho g^2 \zeta_0^{\,2} h C_\Lambda \cdot \left[(1 + C_{B0} - C_{C0}\cos k_0 B)\frac{\tanh k_0 h}{k_0 h} + \sum_{m=1}^{\infty} (C_{Bm} - C_{Cm}\cosh k_m B)\frac{\tan k_m h}{k_m h} \right] \exp(-i2\sigma t) \tag{55}$$

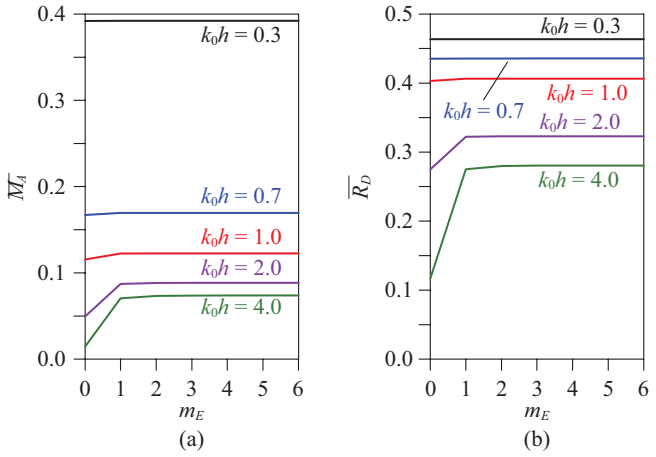

Fig. 2. The convergent speed of the hydrodynamic added mass and radiation damping as a function of m_E and k_0h (G = 1.0 + 0.5i; B/L = 0.25) (a) $\overline{M_A}$; (b) $\overline{R_D}$.

IV. THE HYDRODYNAMIC ADDED MASS AND RADIATION DAMPING

As described in the preceding section, the hydrodynamic added mass M_A and radiation damping R_D can be derived to the dimensionless forms $\overline{M_A}$ and $\overline{R_D}$, respectively (Eqs. (52)-(53)). However, both $\overline{M_A}$ and $\overline{R_D}$ still include an infinite series. For a practical implementation, these series terms are summed until convergent results are obtained. In Fig. 2, the variation of convergence of $\overline{M_A}$ and $\overline{R_D}$ is plotted versus the number of terms m_E for various values of k_0h at G = 1.0 + 0.5i and B/L = 0.25. The infinite series is observed to make a low contribution until k_0h is increased to a certain value, indicating that evanescent waves are important in the deep water region. Generally, a highly convergent speed is obvious as m_E increases for each value of k_0h, and the variation approximates a constant as $m_E \geq 3$. To reduce truncation error, the summation process is terminated when the following condition is satisfied for all the studied examples:

$$\left| \frac{Val_{m_E} - Val_{m_E-1}}{Val_{m_E}} \right| < 10^{-9} \tag{56}$$

where Val_{m_E} denotes a m_E-term summation of a physical quantity. Fig. 3 presents the dimensionless added mass and radiation damping as a function of B/L for various values of k_0h at G = 1.0 + 0.5i. The variations of $\overline{M_A}$ (Fig. 3(a)) and $\overline{R_D}$ (Fig. 3(b)) for all k_0h are oscillating curves (i.e., with periodically occurring local maximum and minimum values) as B/L is increased. Furthermore, the variation period is close to 0.5 B/L. The difference between the local maximum value and local minimum value decreases when k_0h is

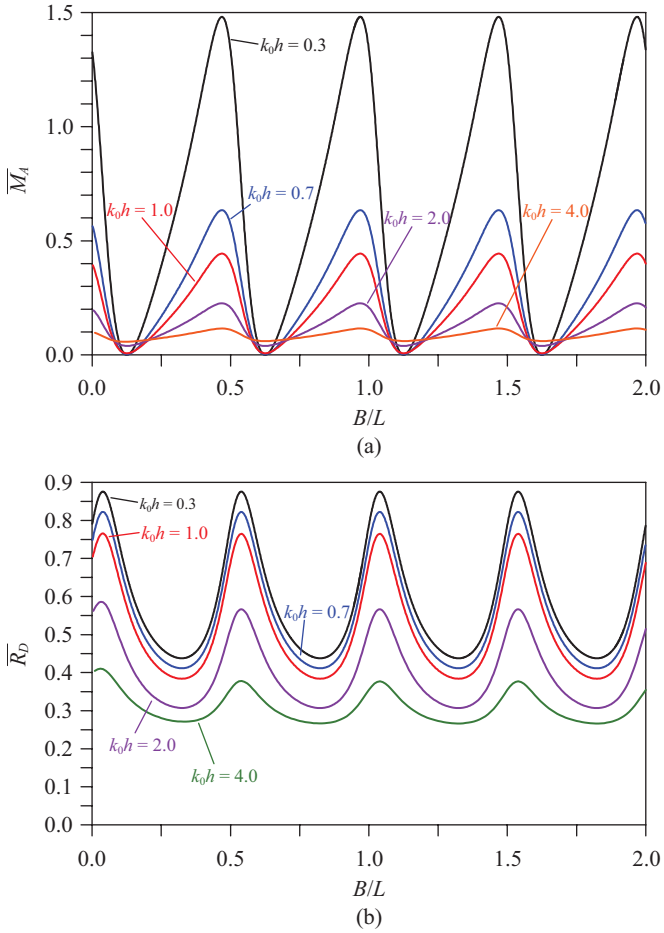

Fig. 3. Variations in the hydrodynamic added mass and radiation damping as a function of B/L and k_0h (G = 1.0 + 0.5i) (a) $\overline{M_A}$; (b) $\overline{R_D}$.

increased. In other words, variations in $\overline{M_A}$ and $\overline{R_D}$ are continuously reduced as k_0h is increased; i.e., $\overline{M_A}$ and $\overline{R_D}$ approximate constants as B/L increases in the deep-water region.

V. THE POROUS-PLATE RESPONSE

Based on linear wave theory, the porous-plate response in this study is a steady-state harmonic motion. We investigated the variation of displacement amplitude Λ for the present converter. Fig. 4 presents the dimensionless amplitude $|\Lambda|/\zeta_0$ as a function of B/L for several values of k_0h at G = 1.0 + 0.5i, $\overline{M_v}$ = 2.5, $\overline{c_v}$ = 0.4, and $\overline{k_v}$ = 1.0. It is evident here that the variation of $|\Lambda|/\zeta_0$ for each k_0h clearly oscillates as B/L is increased; moreover, the period of variation is close to 0.5 B/L. In the cases of low k_0h values, the locations of the maximum $|\Lambda|/\zeta_0$ are found to be near the wave-trapping condition (B/L = n/4 (n = 1, 3, 5, 7, …)). Regardless of the value of k_0h, many motionless phenomena occur at B/L = n/4 (n = 0, 2, 4, 6, …). In other words, when the porous

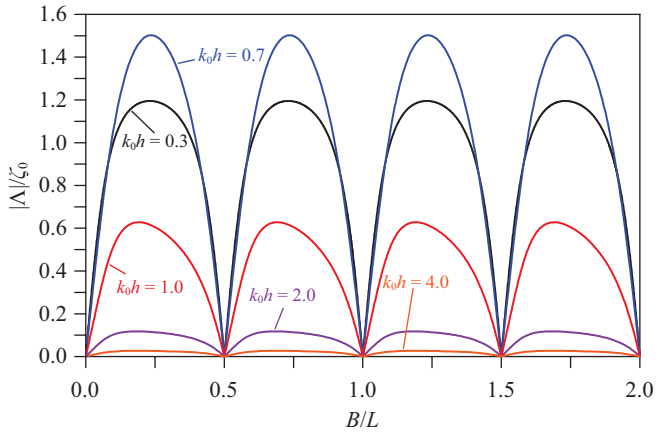

Fig. 4. Response amplitude $|\Lambda|/\zeta_0$ as a function of B/L and k_0h (G = 1.0 + 0.5i; $\overline{M_v}$ = 2.5; $\overline{c_v}$ = 0.4; $\overline{k_v}$ = 1.0).

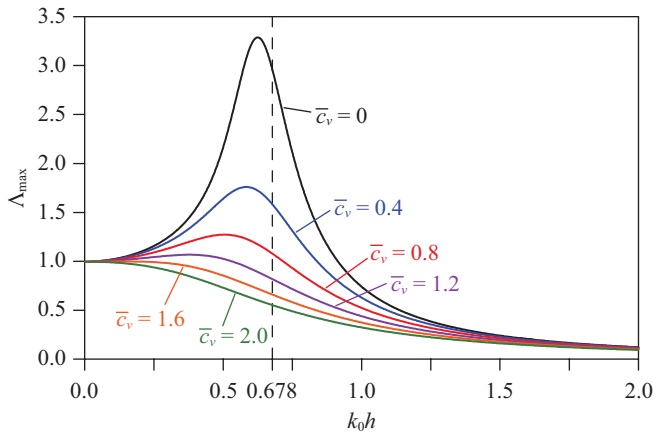

Fig. 5. Maximum response amplitude Λ_{max} as a function of k_0h and $\overline{c_v}$ (G = 1.0 + 0.5i; $\overline{M_v}$ = 2.5; $\overline{k_v}$ = 1.0).

plate is located at a wave antinode, the present converter is an inactive device. Mathematically, the function sin k_0B in Eq. (47) represents motionless phenomena. Under physical conditions, this is a state of static equilibrium. However, Eq. (47) shows that $|\Lambda|/\zeta_0 \to +\infty$ as $\sqrt{a_1^2+b_1^2}\sqrt{a_2^2+b_2^2} \to 0$ (excluding sin k_0B thanh k_0h = 0). In the majority of practical situations, the values of M_v, c_v, k_v [7], G_r, and G_i [24] are finite numbers in the set of positive real numbers. These conditions lead to a value of $\sqrt{a_1^2+b_1^2}\sqrt{a_2^2+b_2^2}$, which is also a finite number in the set of positive real numbers and cannot equal zero based on an analysis of Eqs. (48)-(53). In essence, $|\Lambda|/\zeta_0$ does not approach infinity in practical applications. To determine the maximum value of $|\Lambda|/\zeta_0$ along the k_0h-axis for the same situation, we define a new variable, Λ_{max}, to denote the maximum value of $|\Lambda|/\zeta_0$. Fig. 5 depicts the relationship between Λ_{max} and k_0h for various values of $\overline{c_v}$ at G = 1.0 + 0.5i, $\overline{M_v}$ = 2.5 and $\overline{k_v}$ = 1.0 to delimit the scope of the application of this solution.

The pattern observed here is similar to the variation of the dynamic magnification factor in a SDOF system under a harmonically varying load. The results indicate that Λ_{max} decreases as $\overline{c_v}$ is increased because the damping property in this system absorbs energy and so reduces motion. As described above, the value of Λ_{max} or $|\Lambda|/\zeta_0$ cannot trend toward infinity, even when $\overline{c_v}$ = 0. A physical phenomenon is called resonance, i.e., a property encountered when the frequency of the applied loading equals the undamped natural vibration frequency of the system. In this case, the result suggests that the resonant condition is satisfied when $k_0h \approx$ 0.678. For a damped system, the peak value of Λ_{max} occurs at a value of k_0h slightly less than the resonant k_0h value or low damping values.

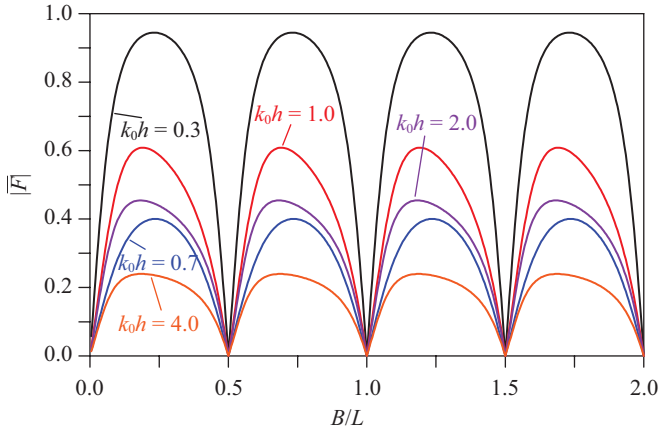

Fig. 6. The amplitude of wave-exerted force as a function of B/L and k_0h (G = 1.0 + 0.5i; $\overline{M_v}$ = 2.5; $\overline{c_v}$ = 0.4; $\overline{k_v}$ = 1.0).

VI. THE WAVE-EXERTED FORCE

We next address the wave-exerted force, $F(t)$, which is expressed as a complex-valued function by Eq. (54). We observe that the variation of $F(t)$ is harmonic along the t-axis; hence, the modulus of $F(t)$ represents the amplitude of the harmonic loading. Defining $\overline{F} = F(t)/\rho g\zeta_0 h$ as the dimensionless $F(t)$, we plot the amplitude of $\overline{F}$ as a function of B/L for several values of k_0h at G = 1.0 + 0.5i, $\overline{M_v}$ = 2.5, $\overline{c_v}$ = 0.4 and $\overline{k_v}$ = 1.0 in Fig. 6. Moreover, the calculated implementation satisfies the truncation condition (Eq. (56)). The location of the maximum is found to be near the wave-trapping condition. The pattern of curves in Fig. 6 is similar to that in Fig. 4; furthermore, a state of static equilibrium still occurs at $B/L = n/4$ (n = 0, 2, 4, 6, …). As described previously, a state of static equilibrium is the reason

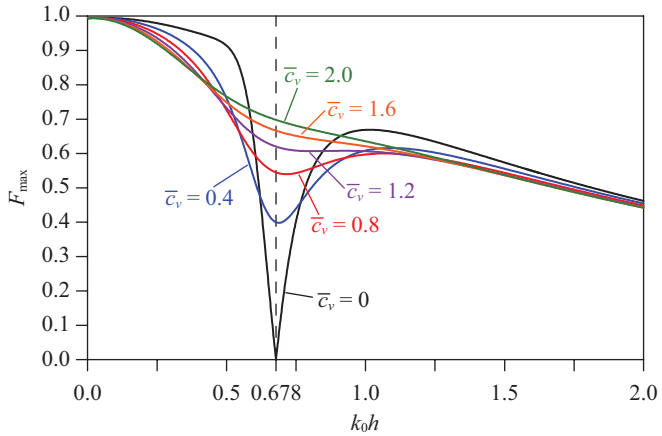

Fig. 7. The maximum amplitude of wave-exerted force as a function of k_0h and $\overline{c}_v$ (G = 1.0 + 0.5i; $\overline{M}_v$ = 2.5; $\overline{k}_v$ = 1.0).

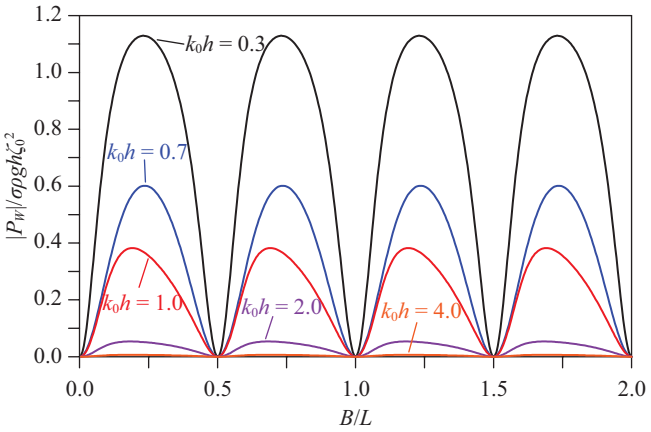

Fig. 8. The amplitude of instantaneous power as a function of B/L and k_0h (G = 1.0 + 0.5i; $\overline{M}_v$ = 2.5; $\overline{c}_v$ = 0.4; $\overline{k}_v$ = 1.0).

for the motionless phenomenon when the porous plate is located at a wave antinode in this system. Again, we define a new variable, F_{max}, to represent the maximum value of $\overline{F}$ for every curve in Fig. 6. As illustrated in Fig. 7, the obvious minimum value of F_{max} occurs at a k_0h value that is slightly more than the resonant k_0h value for low damping values, especially at $\overline{c}_v$ = 0. This is a resonant phenomenon in the $\overline{c}_v$ = 0 case that vanishes as $\overline{c}_v$ increases to a certain value. This phenomenon occurs because a simple harmonic motion (SHM) is allowed to occur without applied loading in an undamped SDOF system. In contrast, a damped SDOF system requires applied loading to avoid a calm response.

VII. THE INSTANTANEOUS POWER

After calculating $F(t)$ and Λ, the instantaneous power $P_W(t)$ is easy to obtain because the product of $F(t)$ and $U_v(t)$ ($=-i\sigma\Lambda e^{-i\sigma t}$) defines the value of $P_W(t)$ (see Eq. (55)). Fig. 8 plots the amplitude of $P_W(t)$ as a function of B/L for several values of k_0h at G = 1.0 + 0.5i, $\overline{M}_v$ = 2.5, $\overline{c}_v$ = 0.4 and $\overline{k}_v$ = 1.0. Expectably, the variation of $|P_W|/\sigma\rho g h\zeta_0^2$ also oscillates along the B/L-axis, and the curves in Figs. 4 and 6 both follow this pattern.

Fig. 8 displays the many local maximum values for each k_0h. The local maximum $|P_W|/\sigma\rho g h\zeta_0^2$ occurs as $B/L \approx n/4$ (n = 1, 3, 5, 7, …) (i.e., the porous plate is located near a wave node). Moreover, several previous studies [17, 18, 21-23] have indicated that wave trapping occurs under the same conditions. Unlike the fixed porous plate, the original porous plate properties (i.e., friction and phase shift) and the PTO mechanism contribute to the absorption of wave energy. Therefore, via a wave-trapping phenomenon, the present converter effectively transforms wave energy into mechanical energy. $P_{W\,max}$ denotes the maximum amplitude

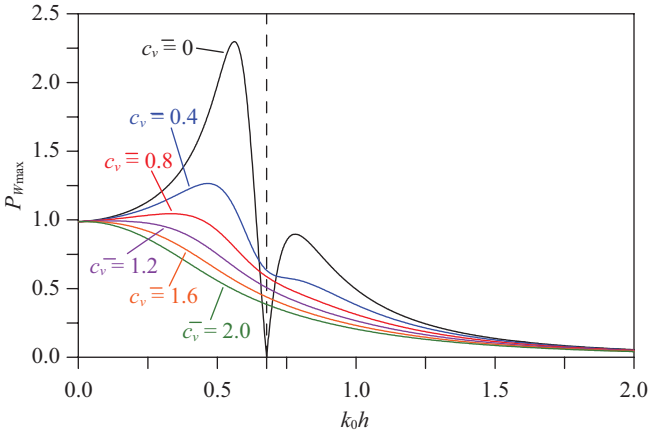

Fig. 9. The maximum amplitude of instantaneous power as a function of k_0h and $\overline{c}_v$ (G = 1.0 + 0.5i; $\overline{M}_v$ = 2.5; $\overline{k}_v$ = 1.0).

of $|P_W|/\sigma\rho g h\zeta_0^2$ for every curve in Fig. 8 to determine the optimal band. Fig. 9 illustrates the influence of varying the dimensionless damping coefficient $\overline{c}_v$ of the converter for the case G = 1.0 + 0.5i, $\overline{M}_v$ = 2.5 and $\overline{k}_v$ = 1.0. The results are shown for converters with the dimensionless damping coefficients $\overline{c}_v$ = 0, 0.4, 0.8, 1.2, 1.6 and 2.0. These results indicate that increasing $\overline{c}_v$ reduces $P_{W\,max}$. Moreover, no power generation occurs at the resonance k_0h value in the undamped case (corresponding to $\overline{c}_v$ = 0) because $F(t)$ = 0 in the same situation (see Fig. 7). Despite the high power available in the undamped case, the bandwidth between the maximum and null values is rather narrow.

VIII. CONCLUSIONS

This study analyzes the interaction between a PTPWEC and a gravity wave train. The PTPWEC transforms wave

energy into mechanical energy using a wave-absorbing chamber containing a vertical porous plate. The current investigation couples linear wave theory with a SDOF system to simulate this system.

These results imply that the width of the wave-absorbing chamber B significantly affects the performance at a fixed value of the dimensionless wavenumber k_0h. Moreover, as B is increased, the value of the hydrodynamic added mass, the radiation damping, the porous-plate response, the wave-exerted force, and the instantaneous power all vary periodically. The maximum values occur when the porous plate is established near a wave node (i.e., near wave-trapping conditions). In contrast, a null situation occurs when the porous plate is established at a wave antinode. In damped systems, the peak value of porous-plate response and instantaneous power is found at a k_0h value that is slightly less than the resonant k_0h value for low damping values, and the damping absorbs wave energy, thereby reducing performance.

REFERENCES

1. Agnon, Y. and Mei, C. C., "Slow-drift motion of a two-dimensional block in beam seas," *Journal of Fluid Mechanics*, Vol. 151, No. 1, pp. 279-294 (1985).
2. Brooke, J., *Wave Energy Conversion*, Elsevier Science, New York (2003).
3. Caska, A. J. and Finnigan, T. D., "Hydrodynamic characteristics of a cylindrical bottom-pivoted wave energy absorber," *Ocean Engineering*, Vol. 35, No. 1, pp. 6-16 (2008).
4. Chwang, A. T., "A porous-wavemaker theory," *Journal of Fluid Mechanics*, Vol. 132, No. 1, pp. 395-406 (1983).
5. Chwang, A. T. and Dong, Z., "Wave-trapping due to a porous plate," *Proceedings of the 15th ONR Symposium on Naval Hydrodynamics*, Hamburg, Germany, pp. 407-417 (1984).
6. Chwang, A. T. and Li, W., "A piston-type porous wavemaker theory," *Journal of Engineering Mathematics*, Vol. 17, No. 4, pp. 301-313 (1983).
7. Clough, R. W. and Penzien, J., *Dynamics of Structures*, Second Ed., McGraw-Hill Inc., New York (1993).
8. Cruz, J., *Ocean Wave Energy: Current Status and Future Prepectives*, Springer, Berlin (2008).
9. Duckers, L., "Wave energy," in: Boyle, G. (Ed.), *Renewable Energy: Power for a Sustainable Future*, Second Ed., Oxford University Press, New York, pp. 297-340 (2004).
10. Falnes, J., "A review of wave-energy extraction," *Marine Structures*, Vol. 20, No. 4, pp. 185-201 (2007).
11. Flocard, F. and Finnigan, T. D., "Laboratory experiments on the power capture of pitching vertical cylinders in waves," *Ocean Engineering*, Vol. 37, No. 11-12, pp. 989-997 (2010).
12. International Energy Agency, *Energy Prices and Taxes-1994*, IEA/OECD, Paris (1994).
13. Isaacson, M., Baldwin, J., Allyn, N., and Cowdell, S., "Wave interactions with perforated breakwater," *Journal of Waterway, Port, Coastal, and Ocean Engineering*, Vol. 126, No. 5, pp. 229-235 (2000).
14. Korde, U. A., "Performance of a wave energy device in shallow-water nonlinear waves: part I," *Applied Ocean Research*, Vol. 19, No. 1, pp. 1-11 (1997).
15. McCormick, M. E., *Ocean Wave Energy Conversion*, Dover Publications Inc., New York (2007).
16. Panicker, N. N., "Power resource estimate of ocean surface waves," *Ocean Engineering*, Vol. 3, No. 6, pp. 429-439 (1976).
17. Sahoo, T., Lee, M. M., and Chwang, A. T., "Trapping and generation of waves by vertical porous structures," *Journal of Engineering Mechanics*, Vol. 126, No. 10, pp. 1074-1082 (2000).
18. Twu, S. W. and Lin, D. T., "On a highly effective wave absorber," *Coastal Engineering*, Vol. 15, No. 4, pp. 389-405 (1991).
19. Vicinanza, D. and Frigaard, P., "Wave pressure acting on a seawave slot-cone generator," *Coastal Engineering*, Vol. 55, No. 6, pp. 553-568 (2008).
20. Wang, K.-H. and Ren, X., "Water waves on flexible and porous breakwaters," *Journal of Engineering Mechanics*, Vol. 119, No. 5, pp. 1025-1047 (1993).
21. Wang, K.-H. and Ren, X., "An effective wave-trapping system," *Ocean Engineering*, Vol. 21, No. 2, pp. 155-178 (1994).
22. Yip, T. L. and Chwang, A. T., "Perforated wall breakwater with internal horizontal plate," *Journal of Engineering Mechanics*, Vol. 126, No. 5, pp. 533-538 (2000).
23. Yip, T. L., Sahoo, T., and Chwang, A. T., "Trapping of surface waves by porous and flexible structures," *Wave Motion*, Vol. 35, No. 1, pp. 41-54 (2002).
24. Yu, X. and Chwang, A. T., "Wave-induced oscillation in harbor with porous breakwaters," *Journal of Waterway, Port, Coastal, and Ocean Engineering*, Vol. 120, No. 2, pp. 125-144 (1994).
25. Yueh, C.-Y. and Chuang, S.-H., "The reflection of normal incident waves by absorbing-type breakwaters," *China Ocean Engineering*, Vol. 23, No. 4, pp. 729-740 (2009).
26. Zhu, S. and Chwang, A. T., "Investigations on the reflection behaviour of a slotted seawall," *Coastal Engineering*, Vol. 43, No. 2, pp. 93-104 (2001).